J Mater Sci (2008) 43:7035–7046
DOI 10.1007/s10853-008-3030-2

Hierarchical description of deformation in block copolymer TPEs

Mohit Mamodia · Kishore Indukuri · Edward T. Atkins · Wim H. De Jeu · Alan J. Lesser

Received: 24 June 2008 / Accepted: 30 September 2008 / Published online: 30 October 2008

Abstract We report on the deformation behavior of commercially relevant lamellar and cylindrical tri-block copolymers poly (styrene-*b*-ethylene-co-butylene-*b*-styrene) (SEBS) with two different compositions. The structural changes that occur at various length scales have been studied using a simultaneous small- and wide-angle X-ray scattering (SAXS/WAXS) during uni-axial tensile deformation of the polygrain samples. SAXS provides information about changes that occur upon deforming the glassy cylindrical or lamellar PS domains. WAXS, on the other hand, is sensitive to the crystallographic structure of the rubbery mid-block. Deformation calorimetry has been used to determine the energetics involved. The combined results from the various techniques indicate that the deformation takes place in three stages. First, at small strains, dilation occurs in the rubbery phase. At intermediate strains, the hard lamellar or cylindrical domains undergo micro-buckling, which is associated with a downturn in the stress–strain curve. Finally, we interpret that at higher strains, the bent lamellar/cylindrical domains rotate in the stretching direction resulting in a significant shear on the rubbery mid-block. This in turn leads to strain-induced crystallization in these materials. Although we could not prove it by WAXS, deformation calorimetry (which is more sensitive than the WAXS) was utilized to show its presence.

M. Mamodia · K. Indukuri · E. T. Atkins · W. H. De Jeu · A. J. Lesser (✉)
Department of Polymer Science and Engineering, University of Massachusetts, Amherst, USA
e-mail: ajl@polysci.umass.edu

Introduction

A well-known class of thermoplastic elastomers (TPEs) consists of tri-block copolymers with glassy domains of atactic polystyrene (aPS) within an elastomeric matrix [1]. Depending on the composition, these materials' microphase separate into nano-structures of spheres, cylinders, or lamellae. In addition a structural hierarchy develops because they nucleate and grow into randomly oriented grains of micron size when cooled from melt or cast from a solution. The morphology and deformation behavior of these materials have been widely studied [2–15]. Significant work on deformation behavior has been done on both highly oriented 'single-crystal' specimens [2–7, 11, 13–15] as well as on polygrain structures [8, 12, 16, 17]. Highly oriented poly (styrene-*b*-butadiene-*b*-styrene) (SBS) TPEs were studied by Keller and coworkers [15] for their deformation behavior at low to moderate strains using SAXS, transmission electron microscopy (TEM), and Birefringence. These studies revealed several important structural features that occur at small to moderate deformations. The deformation behavior at large strains was studied by Godovskii and coworkers [18] using SAXS and deformation calorimetry.

For oriented lamellar and cylindrical micro-structures deformation orthogonal to the orientation is accompanied by a transformation into a 'zig-zag' structure in real space. Longitudinal deformation, on the other hand, results in the breakdown of the cylindrical and lamellar domains. Macroscopically isotropic TPEs which contain random distribution of grains consisting of oriented block domains indicate the formation of a chevron pattern at high strains [8, 12]. However, most of these studies are restricted to two dimensions (2-D) and do not elucidate the full 3-D deformation. The 'zig-zag' and chevron patterns have been

modeled by Read et al [19]. These studies show that orthogonal deformation of multi-layered structures causes initially a sinusoidal buckling of cylinder/layers, which at higher strains develops into a chevron texture. In addition, the buckling instability corresponds to the sharp turn over in the stress–strain curves. Thomas and coworkers [4] have observed dilation of the rubbery phase, at small strains, along the stretching direction (SD) in oriented cylindrical systems. However, such an effect was not seen for perpendicular deformation of oriented lamellar systems [13]. Most studies have focused on the structural changes occurring in the hard PS domains and less attention has been given to the soft rubbery matrix.

The majority of research so far has been on SBS or styrene-isoprene-styrene (SIS) systems, both of which have non-hydrogenated elastomeric mid-blocks. However, commercial interest is mainly in the hydrogenated versions, i.e. SEBS and styrene-*b*-ethylene-propylene-*b*-styrene (SEPS) because of their improved resistance to degradation. Increasing or decreasing the number of ethyl or propyl branches can make the mid-block completely amorphous or more crystallizable, respectively [20, 21]. In the case of crystallization another length scale (of the crystallites) comes into play in addition to the length scale of cylinder and lamellar domains. The objective of this paper is to investigate and compare the structural changes that occur at the different length scales, upon deformation of two commercial SEBS tri-block copolymers that phase separate into lamellar or cylindrical morphology and a polygrain structure. The difference in morphology will be related to the changes in the uniaxial tensile response and behavior in deformation calorimetry.

Experimental

Materials and sample preparation

The material used in this study is a SEBS triblock copolymer provided by Kraton Polymers, U. S. LLC, commercially known as KP16, but will be referred as SEBS-30 throughout the paper. The number '30' refers to the weight fraction of atactic PS at the end blocks (15% PS on each block). The number-average molecular weight (M_n) as determined by GPC is 94 kg/mol with a poly-dispersity index (M_w/M_n) of 1.08. Thick films (0.5–1 mm) for mechanical and morphological characterization were prepared by solution casting in a petri dish. The block copolymer was first dissolved in toluene to obtain a 5 wt% by volume solution. Solvent evaporation occurred over a period of 8–10 days at room temperature. The film was then dried at 45 °C for 6 h to remove the excess solvent. The SEBS-30 system formed a lamellar morphology, and will be referred to as SEBS-30-lam throughout the paper. The SEBS-30 system was also cast in cyclohexane, in which case it formed a different morphology, cylindrical (SEBS-30-cyl).

Characterization and testing

Simultaneous SAXS/WAXS

SAXS and WAXS were done using an in-house setup from Molecular Metrology Inc. It uses a 30 W micro-source (Bede) with a 30 × 30 μm^2 spot size matched to a Max-flux® optical system (Osmic) leading to an almost parallel beam of monochromatic CuK_α radiation (wavelength $\lambda = 0.154$ nm). After passing beam-defining and guard pinholes the beam with a diameter of about 0.5 mm enters the sample chamber. The SAXS intensity is collected by a two-dimensional gas-filled wire detector (mesh size 120 μm) at a distance of 120 cm. A beam-stop of diameter 0.7 mm in front of the detector has in its center a photo-diode allowing monitoring the intensity of the direct beam. WAXS is performed using an image plate with a hole in its center positioned in the sample chamber at the desired distance from the sample (usually about 13 cm). The whole system is evacuated. The angular range for SAXS (determined by the beamstop and the size of the detector) covers a wave vector range $0.09 < q < 1.5$ nm^{-1} in which $q = (4\pi/\lambda)\sin\theta$, 2θ being the scattering angle. This corresponds to dimensions between 4 and 70 nm. The actual distance to each detector has been calibrated using the accurately know reflections from silver behenate and tricosane for SAXS and WAXS, respectively. Unless dictated differently the scattering patterns were recorded at room temperature over a period of 1 h. The 2-D scattering patterns will be presented with a logarithmic intensity scale. The peak positions for the first- and second-order peaks have been determined from the local maxima in the linear scale. We have checked that the background does not influence the peak position.

Mechanical testing and thermal analysis

Monotonic tensile tests were performed at room temperature on an Instron 5800 tensile testing machine using the ASTM D1708 test geometry (gauge length = 22 mm) at a strain rate of 0.45 mm/mm/min. The strain is expressed in percentage values (i.e. strain% = $(L/L_o) \times 100$). To determine the degradation temperature of the block copolymers thermo-gravimetric analysis (TGA) was performed using a TGA2950 (TA Instruments®) for samples of 7–8 mg at a heating rate of 10 °C/min. Differential scanning calorimetry (DSC) was performed using a DSC Q1000 (TA Instruments®) at a scan rate of 5 °C/min.

Deformation calorimetry

To investigate the enthalpic versus entropic nature of deformation and to determine any strain-induced crystallization, deformation calorimetry was carried out. In this method the incremental work (ΔW), absorbed heat (ΔQ), and hence the internal energy changes (ΔU) are measured during deformation as described elsewhere [21–23]. The calorimeter has been used previously to study the heat and internal energy changes in strain-crystallizing natural rubber [24, 25] and thermoplastic elastomers [21]. We used ASTM D1708 test geometry at a strain rate of 1.08 mm/mm/min at a temperature of about 25 °C. The internal energy was recorded after two stress–strain cycles.

Results and discussion

Deformation behavior of lamellar block copolymers

Unstretched state and small deformations (strain ≤30%)

SAXS was performed in the geometry illustrated in Fig. 1. The unstretched SEBS-30-lam system (Fig. 2a) shows an isotropic diffraction pattern with a series of rings of decreasing intensity at increasing q-values. This pattern suggests a random distribution of the internally oriented grains. Figure 2b and c shows the shape of the first-order diffraction maximum with a schematic of a grain. These can be compared with Fig. 2d–f for 10% strain. Figure 3a shows 1-D SAXS plots obtained by a full circular integration of Fig. 2a. The plot indicates positions of the diffraction peaks in a ratio of 1:2:3, which illustrates the lamellar morphology. However, from the composition we expect the equilibrium morphology of the SEBS-30 system to be cylindrical. Cylindrical morphology was also seen when prepared from melt state. The lamellar structure observed here is attributed to toluene used for solution-casting, which acts as a selective solvent for styrene. It preferentially swells the styrene domain which changes the morphology from thermodynamic equilibrium to a kinetically trapped lamellar morphology. Such changes in morphology have been observed before [9]. The equilibrium cylindrical morphology is obtained for solution casting from cyclohexane only.

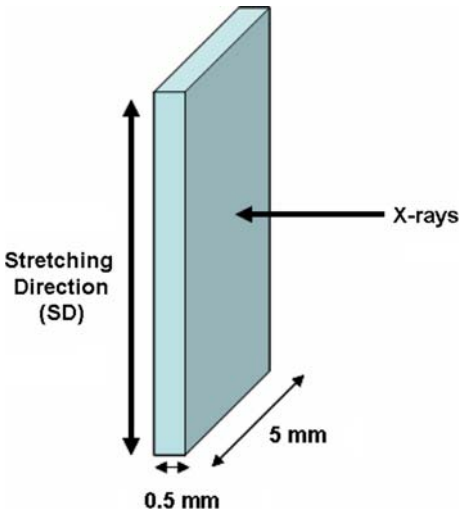

Fig. 1 Geometry of the SAXS experiment

At 5–10% strain a noticeable anisotropy is seen in the SAXS. The first-order maximum transforms from circular to elliptical (compare Fig. 2a, d). The scattering along the meridian axis shifts to smaller scattering angles, while there is hardly a change in the peak positions along the equatorial axis. The variation in the shape of the diffraction pattern is illustrated in Fig. 2b and e. The shift is associated with an increase in the period of the lamellar structures (about 11% dilation) aligned perpendicular to the SD. The region below 5% strain falls in the initial linear elastic region of the stress-extension ratio plot (Fig. 3b). Hence we attribute the deformation in the elastic region initially to stretching of the soft segments (compare Fig. 2c, f). At 10% strain, there is a sharp drop in the stiffness. The extent of dilation along the SD further increases to ~18% at a macroscopic strain of 20%.

Figure 3a includes 1-D SAXS plots for the sample stretched at 20% strain in the direction parallel and perpendicular to the SD. The ratio between the position of the first-order and second-order scattering peaks remains close to 1:2 both parallel and perpendicular to the SD. This indicates that the lamellar packing is preserved.

WAXS pattern in the unstretched state (Fig. 4a) reveals a broad diffuse scattering centered at $q = 14.6\ \mathrm{nm}^{-1}$. The large full-width at half maximum (FWHM), see Table 1, indicates typically short range order only without any indication of crystallinity. However, differential scanning calorimetry shows a melting point at 29 °C and an exotherm of about 16 J/g (~5% crystallinity) on 2nd heating run from below room temperature. No change was observed in the WAXS pattern at small strains (strain ≤50%).

Deformation at intermediate strains (strain ≈50%)

At intermediate strains of about 50% the 2-D SAXS pattern (Fig. 5a) shows a fundamental change. First the elliptical shape changes to a four-point cross. In addition, two strong diffraction spots are seen along the meridian axis. The position of the SAXS measurements on the stress-extension ratio curve is indicated in Fig. 3b. By integrating the 2-D figure over 20° around the cross axes, we obtain the 1-D SAXS intensities shown in Fig. 6 for various strain levels. Note the second-order peaks along the cross axes, which

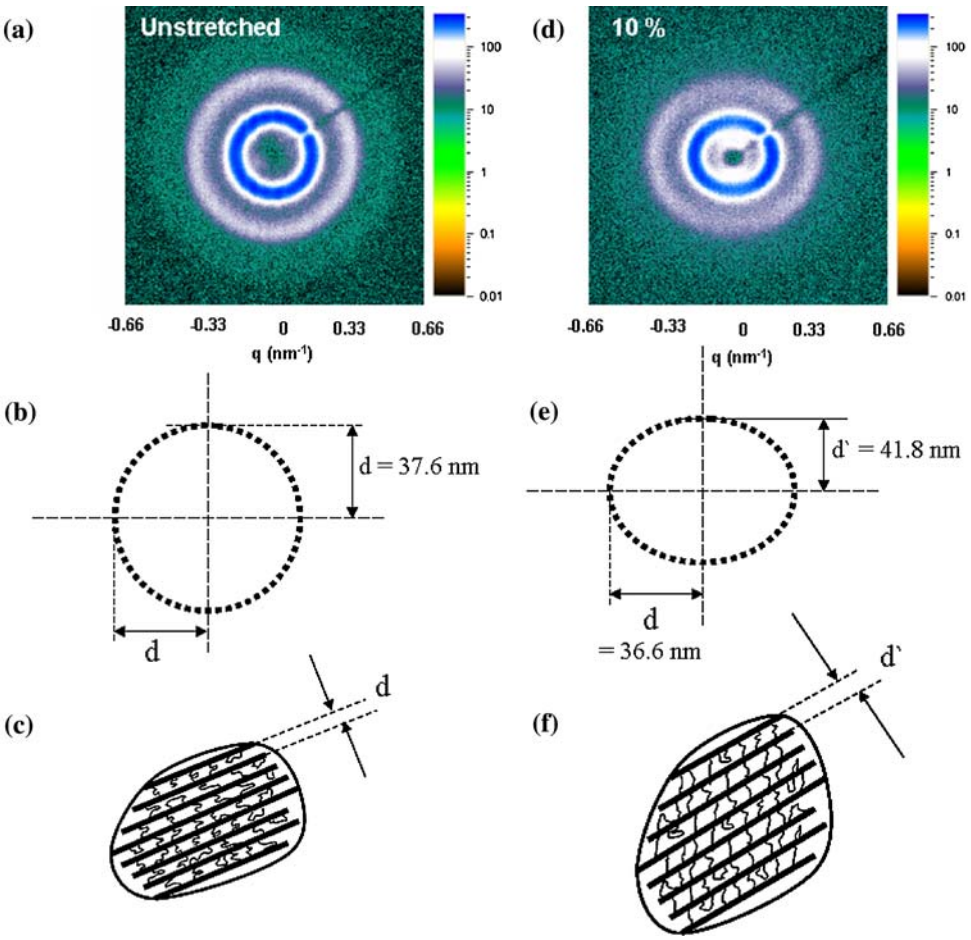

Fig. 2 X-ray results for SEBS-30-lam. SAXS, shape of the first-order diffraction maximum and schematic representation of a grain, in unstretched state (**a**–**c**) and at 10% strain (**d**–**f**)

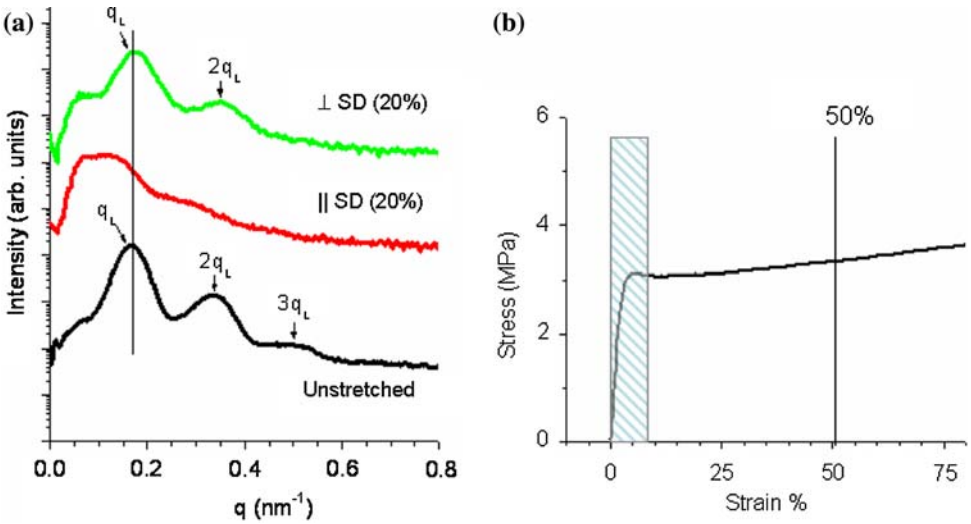

Fig. 3 Results for SEBS-30-lam. **a** 1-D SAXS intensity plots for (from bottom to top) the unstretched state and perpendicular and parallel to the SD at 20% strain (curves are obtained by an integration over 20° along a required direction and are shifted over two decades for clarity), **b** Stress versus extension ratio plot showing the small strain regime

are barely visible in Fig. 5b, can be clearly distinguished in the 1-D plot. A schematic representation of this scattering pattern is given in Fig. 5b. We attribute the cross pattern to the formation of a herringbone/chevron structure by the lamellar sheets. Such structures have been interpreted [19] as a consequence of a micro-buckling instability that occurs in the glassy PS sheets. Following Thomas's work [13] a schematic picture of such a deformation is given in Fig. 5c. Alternatively the lamellar sheets could undergo fragmentation (at small strains) and subsequent rotation (at intermediate to high strains) leading chevron pattern in real space, and thus to a cross pattern in reciprocal space.

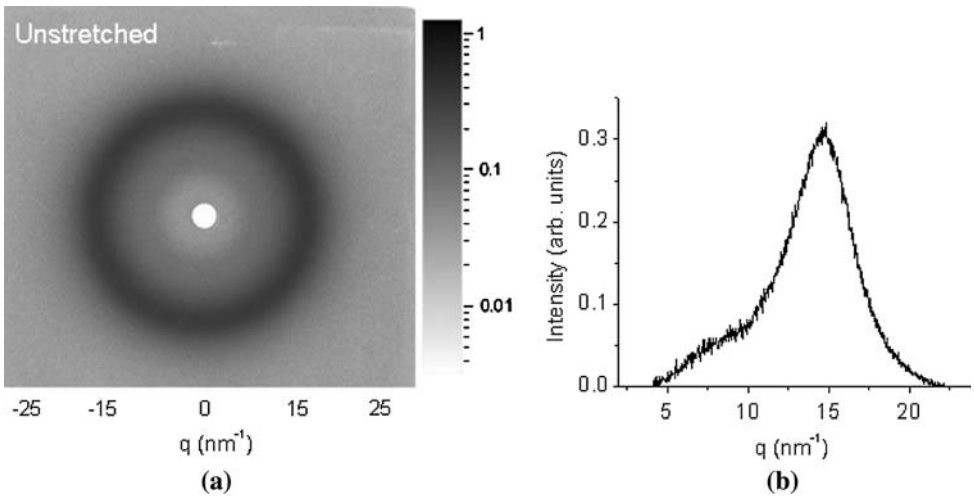

Fig. 4 Results for SEBS-30-lam. **a** WAXS pattern, **b** 1-D WAXS plot (obtained by full circular integration of the 2-D pattern in (**a**)), in the unstretched state

Table 1 WAXS data: d-spacing, full-width at half maximum (FWHM), and corresponding correlation length of the lamellar and cylindrical samples at 0 and 200% strain

Sample	d-spacing (Å)	FWHM (nm^{-1})	Correlation length (Å)
SEBS-30-lam: unstretched	4.26	4.57	13.7
SEBS-30-lam: 200% strain	4.18	4.1	15.3
SEBS-30-cyl: unstretched	4.54	4.6	13.7
SEBS-30-cyl: 200% strain	4.48	4.1	15.3

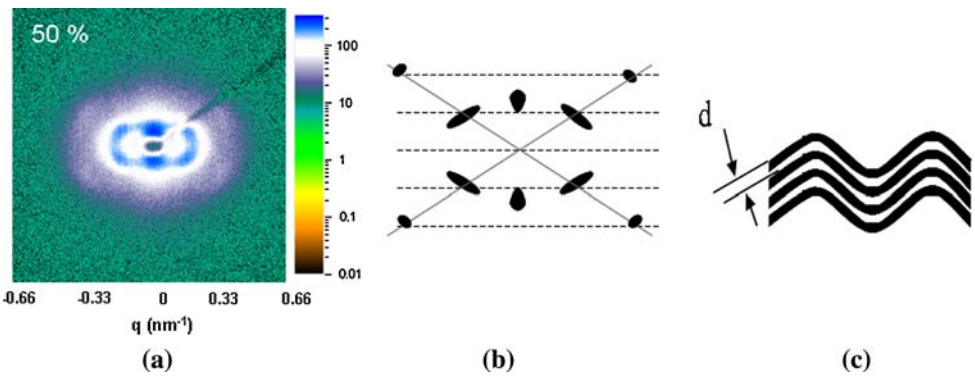

Fig. 5 Results for SEBS-30-lam at 50% strain. **a** 2-D SAXS pattern, **b** schematic representation of (**a**), and **c** schematic representation of micro-buckling of glassy lamellar sheets

The 1-D SAXS plot along the cross axes in Fig. 6 shows that at 50% strain the ratio of first- and second-order peak position is still 1:2. Evidently the lamellar packing is preserved even after micro-buckling suggesting that buckling occurs in a cooperative fashion (i.e. the lamellar sheets in a single grain buckle simultaneously). At a certain critical load (Fig. 3b) the buckling instability is responsible for a sudden drop in the stiffness near 5% strain (apparent yield like behavior). However, there is no way that we can directly monitor this instability with X-ray scattering. Stress relaxation tests were performed both before and after this sudden change in stiffness. Most of the relaxation occurs in first few minutes, i.e. well before the X-ray exposure and very little change is expected during the X-ray measurements. Comparisons are made in the stable regimes that occur before and after the sudden change in stiffness. It is the interpretation of the morphologies, which occur in these regimes, we have used to understand the micro-mechanics of deformation. Note that such real-time studies, feasible with sub-second time-resolved SAXS/WAXS at synchrotron X-ray sources, could shed further light on the issue. There is still no significant change in the WAXS pattern in this intermediate strain regime.

The strong meridonal peaks deserve special attention. In reference 13, meridonal streaks were reported at these positions during the perpendicular deformation of oriented lamellar systems. These were attributed to thin hinged regions where the layers are in a plane perpendicular to the SD with an increased lamellar spacing (compare Fig. 5c). This interpretation cannot be expected to apply in full to our results on polygrain lamellar systems in which the meridonal peaks are strong.

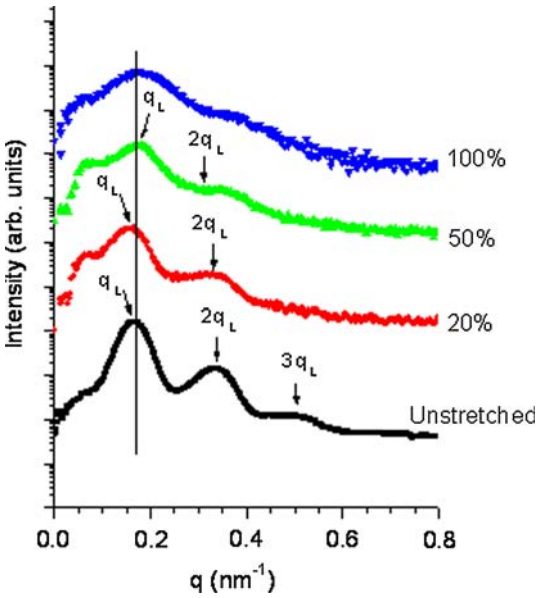

Fig. 6 1-D SAXS plots for SEBS-30-lam obtained by integration over 20° along the cross axes for (from bottom to top) the unstretched state and 20, 50, and 100% strain

We conclude that our results so far on the deformation behavior in lamellar systems only qualitatively tend to agree with the findings of other authors [2–4, 13, 14] on SIS and SBS systems as well as with the model of micro-buckling. This regards especially the strong lamellar peaks along the meridonal axis. Figure 7 shows a 2-D SAXS pattern of SEBS-30-lam with the X-ray beam incident along the plane of the film. A significant anisotropy is observed which we associate with alignment of lamellar sheets as they are stratified in the plane of the as-cast film. Any other possibility would disrupt the isotropy observed when the X-ray beam is along the film normal (Fig. 2a). Given the extension of the arc in Fig. 7, the lamellar sheets can be expected to have a preferred plane of alignment, with a fraction of sheets somewhat tilted out of the plane.

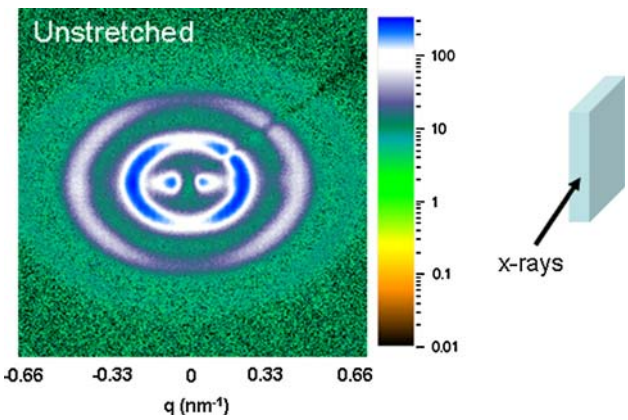

Fig. 7 2-D SAXS pattern for SEBS-30-lam with X-ray beam incident through the thickness of the film in the unstretched state

Such morphology raises questions with regard to the mechanisms of deformation. It is difficult to accept that micro-buckling followed by plastic-hinge formation is the prevalent mechanism when the majority of the sheets are still aligned along the loading direction. Other possibilities should be considered like fragmentation and subsequent rotation of the glassy domains. Further experiments are required to solve this problem and are the subject of future work.

Lamellar systems: deformation at higher strains (strain % >50)

At high levels of strain the 2-D SAXS patterns (Fig. 8a) still show the cross pattern clearly. The opening angle of the cross increases from 141° at 100% strain to 148° at 400% strain. We attribute this increase to a rotation of the bent lamellar sheets in the SD, as illustrated in Fig. 8b. Note that upon going from the unstretched state to 100% strain, the first-order peak positions (along the cross axes) first remain unchanged at smaller q-values (from 0 to 20% strain) to finish at slightly larger ones (see Fig. 6 and Table 2). This suggests that after micro-buckling the lamellar distance decreases even while the rubbery chains are stretched—this is theoretically conceivable when lamellar stacks rotate/tilt and rubbery chains are "sheared" to form shallow angles with the glassy lamellar plane. Also note that up to the highest strains the meridonal peaks remain strong. The WAXS patterns at high strains of Fig. 8d shows that the relative intensity along the equatorial axis increases at the expense of the original diffraction ring. We associate this asymmetry with orientation of rubbery chains. As the glassy lamellar PS sheets rotate, they put a significant shear on the PE/PB matrix; see the schematic in Fig. 8c. The shear-imposed deformation leads to elongation of the PE/PB chains along the SD. If the mid-block is able to crystallize, such a significant deformation could cause strain-induced crystallization. However, the present WAXS patterns provide no evidence for such an effect. The 1-D WAXS intensity plot obtained from the 2-D pattern along the equatorial axis at 200% strain (Fig. 9) also fails to show any crystallization peak. The large FWHM (Table 1) again indicates a short range order.

As a further check of possible strain-induced crystallization, deformation calorimetry was employed which is more sensitive than the present WAXS and has an error margin of 0.1 J/gm. It measures the energy changes upon deformation and hence provides a valuable tool for studying non-linear changes in the internal energy of elastomers/rubbery solids. It has been used effectively to study strain-induced crystallization in natural rubber [24, 25] and polyurethanes [26]. Indukuri and Lesser [21] have performed deformation calorimetry on similar SEBS

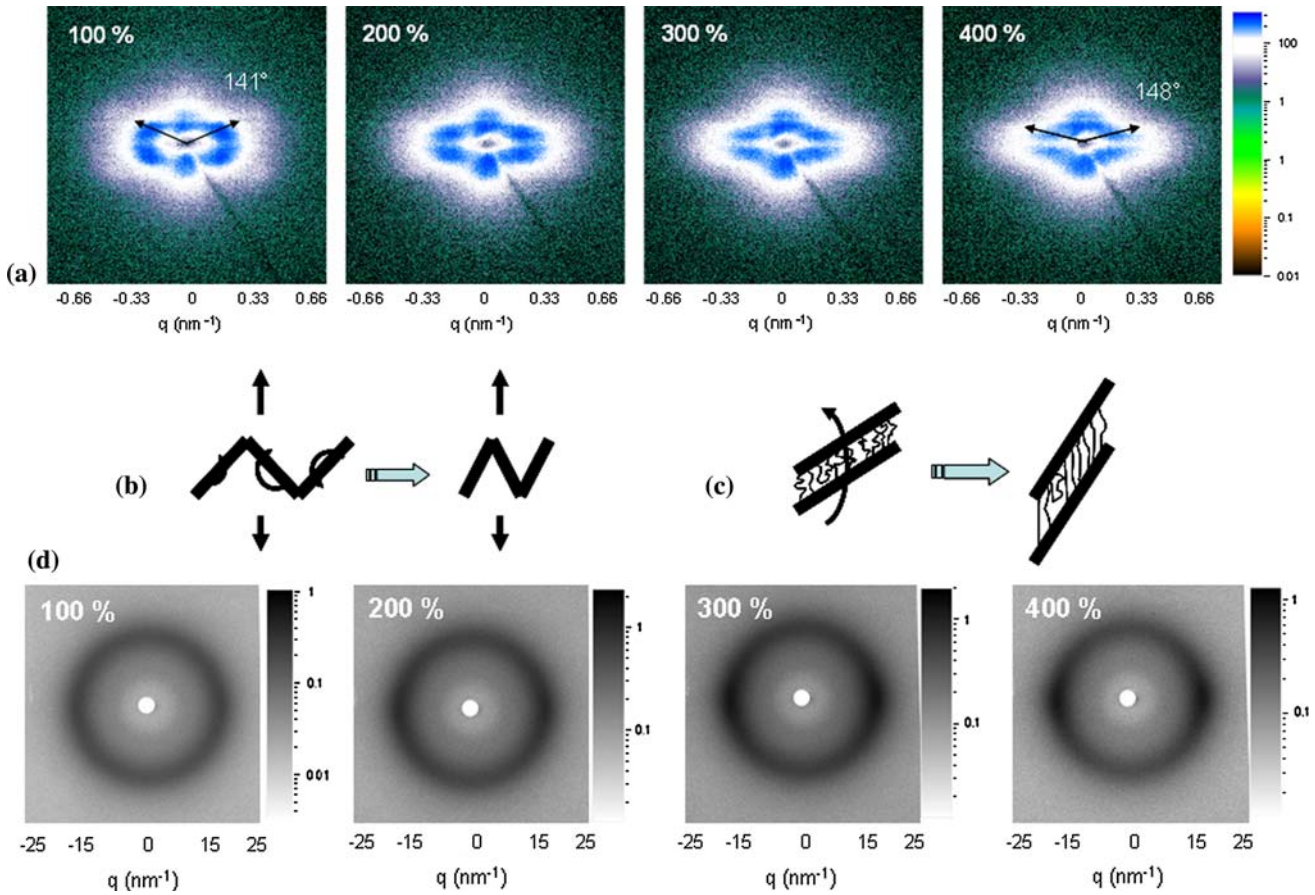

Fig. 8 Results for SEBS-30-lam. **a** 2-D SAXS patterns at 100, 200, 300, & 400% strain (The angle was measured by first creating 2-D SAXS patterns with linear intensity scaling and manually measuring the angle between two sharp spots w.r.t. the center), **b** schematic representation showing rotation of bent PS-sheets, **c** schematic representation showing imposed shear deformation in rubbery phase due to the rotation of PS-domains, **d** corresponding WAXS patterns

Table 2 SAXS data: peak positions for first-, second-order maxima, and d-spacings corresponding to the first peak

Strain %	q_L (nm^{-1})	d-spacing (Å)	$2q_L$ (nm^{-1})
SEBS-30-Lam			
0	0.167	376.0	0.337
20	0.167	376.0	0.333
50	0.181	347.0	0.344
100	0.178	352.8	–
SEBS-30-Cyl			
0	0.235	267.2	0.384
50	0.198	317.2	0.326
100	0.186	337.6	–
200	0.174	360.9	–
20 ($\perp$ to SD)	0.243	258.4	–
20 ($\parallel$ to SD)	0.178	352.8	0.292

tri-block copolymers that shows strain-crystallization when in the mid-block the number of ethylene segments exceeds that of the butylene segments. Figure 10 shows the changes in internal energy (ΔU), along with work exerted on (ΔW) and heat released by the system (ΔQ). For reference the figure also displays the stress-extension ratio plot. The internal energy measurement indicates that as ΔW increases initially, ΔU also increases. However, at about 130% strain the ΔU starts to drop. Such a decrease in ΔU between intermediate and large strains indicates strain-induced crystallization [21, 24]. The internal energy decreases steadily till about 250% strain, after which it again increases. The latter increase in ΔU above 250% strain may be due to the distortion or breaking apart of crystallites at high stress levels (stress-induced de-crystallization). This behavior was observed [24] for natural rubber at strains close to its failure (i.e. strain >650%).

Deformation behavior of cylindrical block copolymers

Unstretched state and deformation at small strains

The 2-D SAXS pattern of an unstretched SEBS-30-cyl system (Fig. 11a) shows a circularly symmetric diffraction

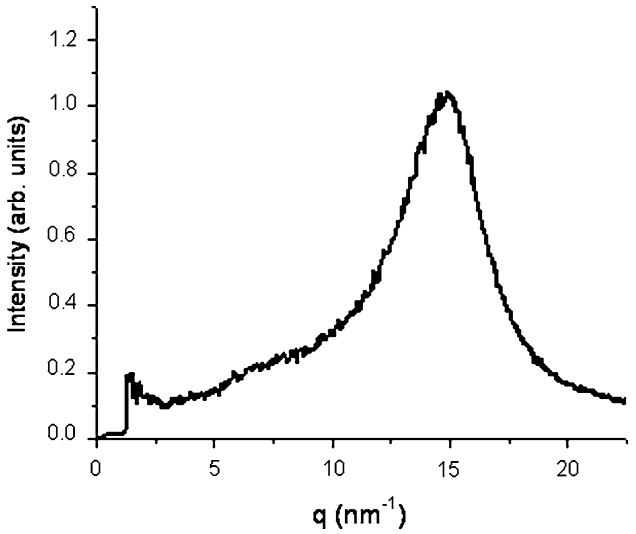

Fig. 9 1-D WAXS intensity plot of SEBS-30-lam at 200% strain obtained by sector integration over an opening angle of 20° along equatorial axis

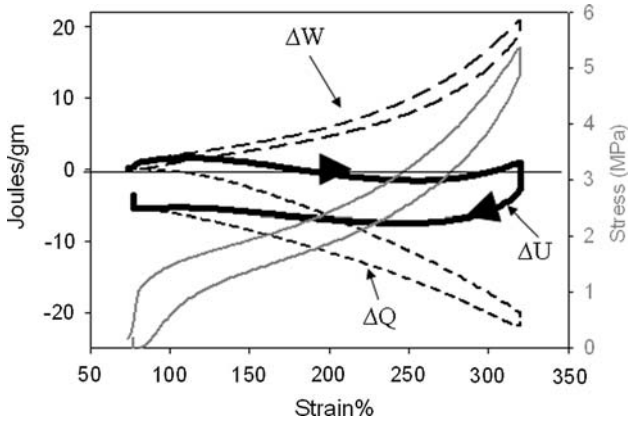

Fig. 10 Deformation calorimetry on SEBS-30-lam

pattern with a series of rings of decreasing intensity at increasing q-values. The 1-D SAXS plot corresponding to this pattern shown in Fig. 12a is obtained by full circular integration. The diffraction peak positions have a ratio of $1{:}\sqrt{3}{:}\sqrt{7}$ indicating a hexagonal packing (cylindrical PS domains in a PE/PB matrix). In addition, the $\sqrt{7}$ peak is superimposed on a broad diffraction ring at $q = 0.69$ nm^{-1}. No peak is seen at $\sqrt{4}$, most probably indicating a close form-factor zero. The 2-D SAXS data support a model of localized regions of parallel PS cylinders packed in a planar hexagonal lattice. These regions are in turn distributed randomly in the plane of the film.

At 20% strain, the first-order maximum of the 2-D SAXS pattern (Fig. 11c) shows a transition from a circle to an ellipse indicating an increase in the periodicity of cylinders aligned perpendicular to the SD. The dilation is about 30%, appreciably larger than for the lamellar system (18%) at the same level of macroscopic strain. In the cylindrical systems, the glassy PS-cylinders are embedded in rubbery matrix which is fully continuous. As a result the system can be easier and further deformed than the lamellar one, in which the rubbery layers are all connected to and separated by glassy PS layers. Transverse loading of relatively stiff PS-sheets will impose a tri-axial state of stress on the rubbery phase. This indicates that the rubbery chains are rather constrained in the lamellar system compared to the cylindrical situation. The state of 20% strain falls in the initial linear elastic region of the stress-extension ratio plot in Fig. 12b. Hence, both for the cylindrical and the lamellar system the deformation in the initial linear region of the stress–strain curve is due to the stretching of rubbery chains. However, the linear elastic region extends further for the cylindrical system (till 20% strain compared to 5% for lamellar system).

Figure 12a includes 1-D SAXS plots for the sample at 20% strain in the direction parallel and perpendicular to the SD. The ratio between the positions of the first two diffraction peaks remains close to $\sqrt{3}$ both parallel and perpendicular to the SD (see Table 2). Hexagonal packing of the cylindrical domains is preserved.

Figure 13 displays WAXS patterns for the SEBS-30-cyl system at various levels of strains. WAXS pattern of the unstretched samples shows an amorphous halo, corresponding to a dimension of 0.46 nm. As in the previous case no indication of crystallinity at room temperature is found.

Deformation at intermediate strains (strains ~50%)

At 50% strain (Fig. 14a) the 2-D SAXS pattern transforms into a four-point cross, however, now without meridonal peaks (see schematic in Fig. 14b). The cross pattern indicates a micro-buckling instability in cylindrical domains. The position of the SAXS measurements on the stress-extension ratio curve is indicated in Fig. 12b. Micro-buckling causes a drop in stiffness which we regard as 'apparent' yield like behavior, just as for the lamellar system. However, for the cylindrical system this drop is more gradual which is attributed to the continuous rubbery matrix where the rubbery chains are less constrained.

The 1-D SAXS plots along the cross axes (Fig. 15) reveals a ratio of first and second peak position ~1.64 (see Table 2). This is still close to $\sqrt{3}$ suggesting that the hexagonal packing is hardly disturbed. The broad diffraction ring at $q = 0.69$ nm^{-1} in unstretched state, has now transformed into a pair of arcs centered along the equator. The arc length decreases with increasing strain. The origin of these diffraction arcs will be discussed below.

Deformation at high strains (strain >50%)

At high strains the opening angle of the cross pattern (Fig. 16) increases from 126° at 100% to 146° at 400%

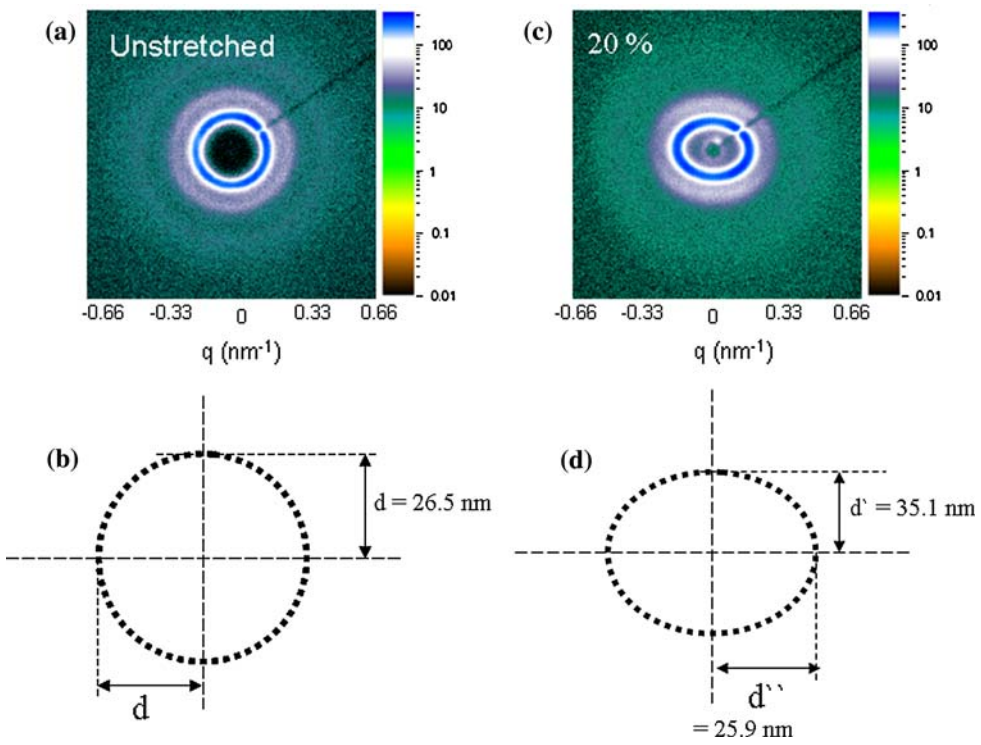

Fig. 11 X-ray results for SEBS-30-cyl. SAXS and shape of the first-order diffraction maximum in unstretched state (**a**, **b**) and at 20% strain (**c**, **d**)

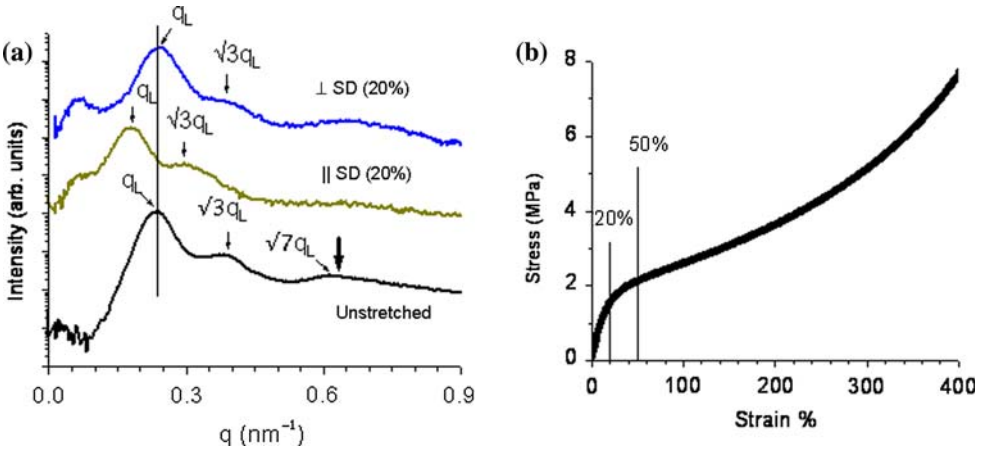

Fig. 12 Results for SEBS-30-cyl. **a** 1-D SAXS intensity plots for (from bottom to top) the unstretched state and perpendicular and parallel to the SD at 20% strain, **b** Stress versus extension ratio plot showing the small and intermediate strain regime

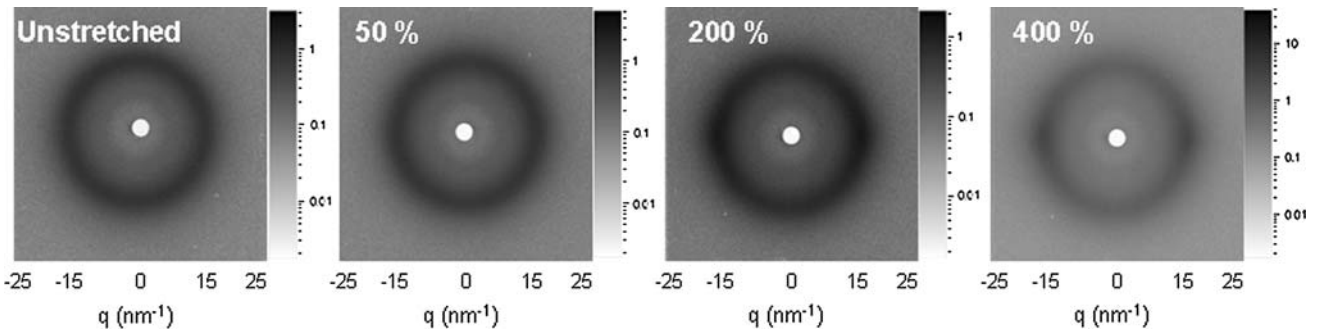

Fig. 13 2-D WAXS patterns of SEBS-30-cyl for the unstretched state and 50, 200, & 400% strain

strain. We attribute this increase with the rotation of bent cylinders toward the SD. The 1-D SAXS plots at strains ≥50% (Fig. 15) indicate a shift of the position of first-order maximum along the cross axes to smaller q-values with increasing strain (see Table 2). The periodicity of the (110) planes of the hexagonal lattice increases to 31.7 nm from

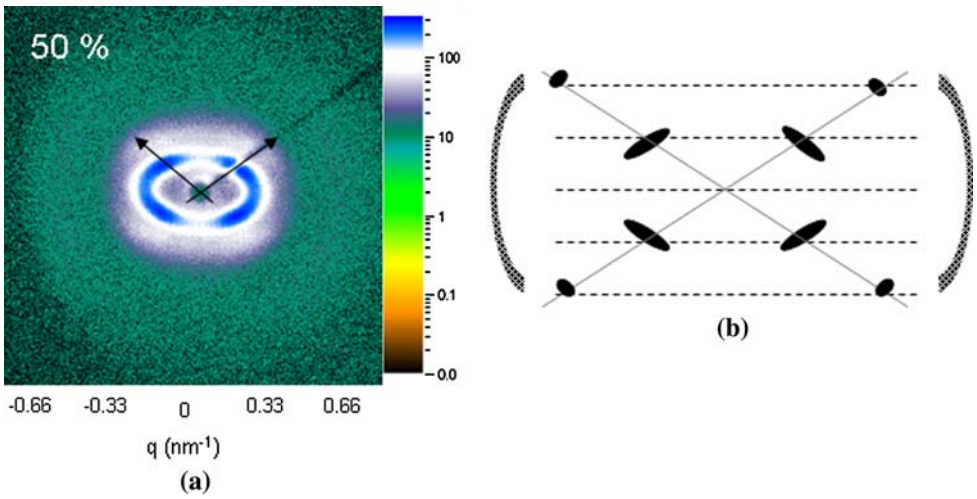

Fig. 14 Results for SEBS-30-cyl at 50% strain. **a** 2-D SAXS pattern, **b** schematic representation of the diffraction pattern in (**a**)

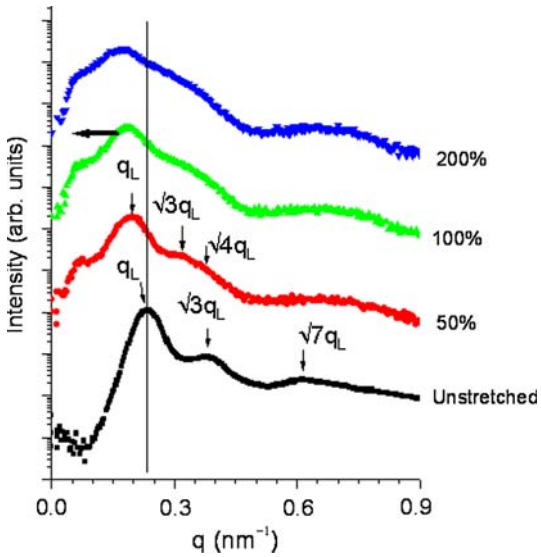

Fig. 15 1-D SAXS intensity plots for SEBS-30-cyl obtained by integration over 20° along the cross axes for (from bottom to top) the unstretched state and 50, 100, and 200% strain

the original value of 26.7 nm at 50% strain and continues to increase for higher strains even after micro-buckling. This behavior differs from the situation in the lamellar system where the rubbery chains are highly constrained and restrict dilation.

At strains >100%, the broad diffraction signal at $q = 0.69$ nm^{-1} has changed into a pair of vertical streaks. This diffraction signals are barely visible at small strain but are seen more clearly at 300% and 400% strain. The 1-D SAXS plot along the equatorial axis in Fig. 17 indicates that its position does not change with strain. This diffraction can be attributed to the secondary maximum of the form-factor scattering [27], i.e. the scattering from an individual cylindrical domain. The diameter of PS cylinders ($2R$) can be calculated from the position of form-factor maxima using the relationship:

$$\frac{4\pi}{\lambda}\sin\left(\frac{\theta_i}{2}\right)R = 4.98,\ 8.364,\ 11.46\ldots \quad \text{for cylinder; } i = 1, 2, 3 \tag{1}$$

where, θ_i is the ith-order particle scattering peak. The diameter of the cylindrical domains turns out to be 14 nm for SEBS-30-cyl. After micro-buckling, the bent cylinders are oriented at some angle to the SD, which will vary from grain to grain. Since the cylinders, oriented perpendicular to SD, have changed their direction, the intensity of this signal diminishes along the meridonal axis. At high strains, most of the cylindrical domains are at a small angle (which is a function of the angle of the kinked region) to the SD resulting in the formation of vertical streaks. The length of the streak can be expected to decrease with increasing orientation of the cylinder axis along the SD.

The rotation of glassy cylindrical domains imposes significant shear on the rubbery matrix orienting PE/PB chains along the SD. The WAXS patterns at high strains of Fig. 13 show that the intensity along the equatorial axis increases at the expense of original diffraction ring, just like the lamellar system. Again, also for SEBS-30-cyl the WAXS does not provide any evidence of strain-induced crystallization. Deformation calorimetry (Fig. 18) on this system reveals that the ΔU initially increases till about 150% strain and then starts to decrease. This decrease indicates also for SEBS-30-cyl strain-induced crystallization. However the ΔU does not show a significant increase at strains >300%, as observed for the lamellar system. This indicates that decrystallization at high strain is absent in cylindrical system. These results further substantiate that the rubbery chains are more constrained in lamellar systems than in cylindrical systems.

We finish this discussion by a short summary of the similarities and differences of the cylindrical and lamellar system. In both cases the elliptical pattern in the SAXS pattern indicates dilation of the rubbery phase at small

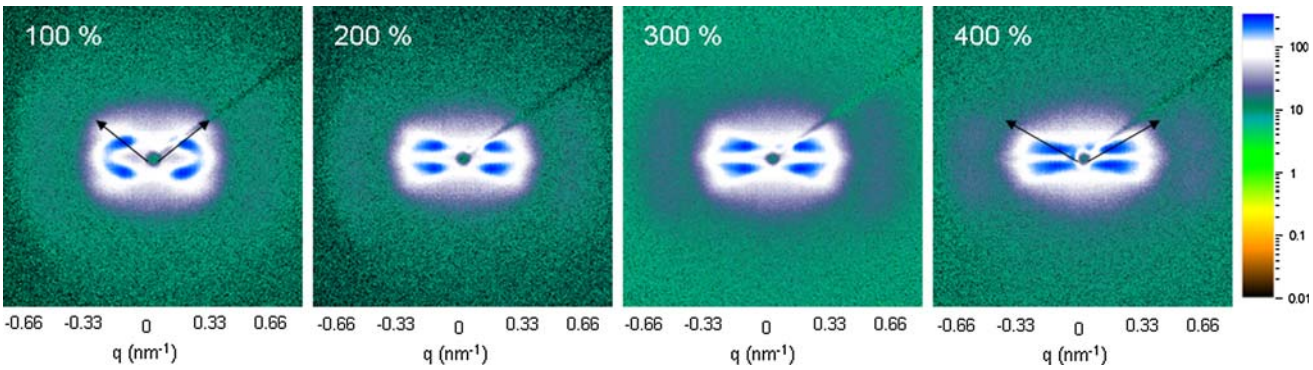

Fig. 16 2-D SAXS patterns of SEBS-30-cyl at 100, 200, 300, & 400% strains

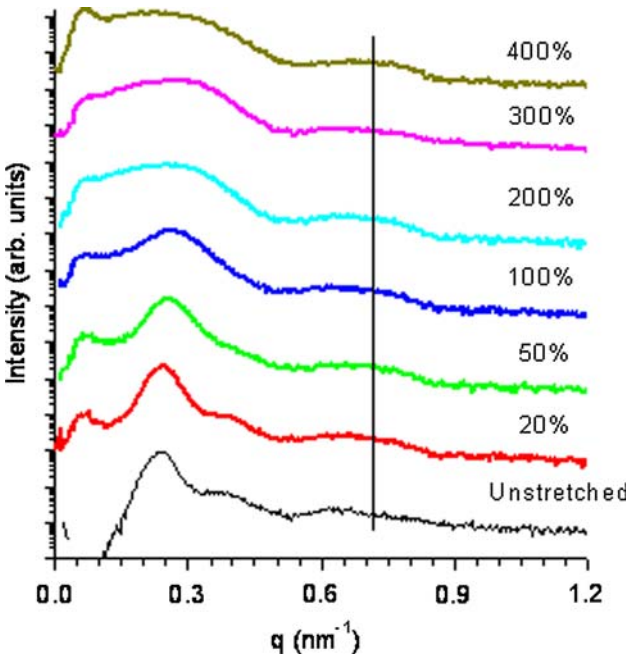

Fig. 17 1-D SAXS intensity plots of SEBS-30-cyl by integration over 20° along the equatorial axis at various strain levels

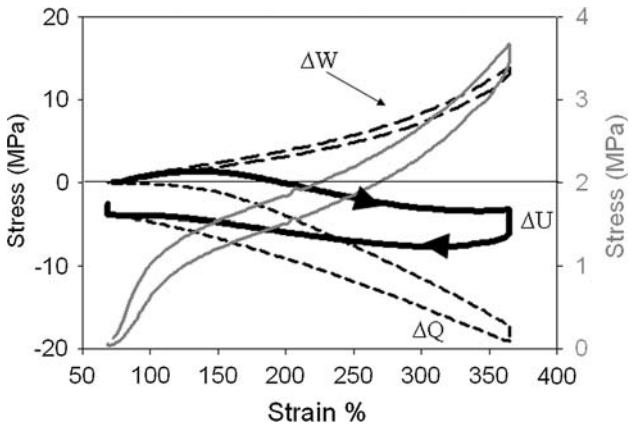

Fig. 18 Deformation calorimetry of SEBS-30-cyl

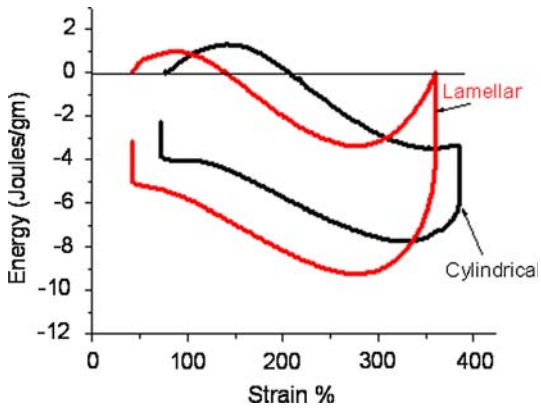

Fig. 19 Internal energy change in SEBS-30-lam and SEBS-30-cyl as obtained from deformation calorimetry

strains, while the four-point cross pattern indicates micro-buckling of the glassy PS-domain after a critical strain. The lamellar system shows additional diffraction spots along the meridonal axis that cannot be fully explained by plastic-hinge formation. The cylindrical system, on the other hand, shows equatorially placed vertical streaks indicating cylinder rotation at higher strains. Figure 19 compares the ΔU changes in the SEBS-30-cyl and SEBS-30-lam systems. In both cases ΔU increases initially and starts to decrease after reaching a maximum at $\sim$150% strain. The decrease in ΔU corresponds to strain-induced crystallization in both morphologies. At higher strains (300% $<$ strain $<$ 400%) the ΔU again shows a significant increase for the lamellar system. The ΔU reaches a minimum for cylindrical system as well, but hardly increases. The sharp increase in the ΔU for lamellar system tentatively attributed to stress-induced de-crystallization. The rubbery chains in lamellar systems are more constrained and the crystals formed at high strain can sustain distortions. The WAXS fails to show any strain-induced crystallization. It might be because of weak signal on an amorphous halo from the amorphous phase.

Conclusions

We have compared the deformation behavior of a cylindrical and lamellar tri-block copolymer at different length scales. The deformation behavior appears to occur in three stages. Dilation of rubbery phase occurs at small strains, followed by micro-buckling at intermediate strains and rotation of the bent cylindrical or lamellar domains in the SD at high strains. Details of the SAXS patterns reveal that the micro-buckling occurs in a cooperative fashion. The rotation at high strains puts significant shear on the rubbery mid-block and is responsible for strain-induced crystallization, as indicated by the internal energy measurement from deformation calorimetry. However, the WAXS fails to show the crystallization. It might be because of a weak signal on an amorphous halo from the glassy PS and amorphous rubbery phase. In the lamellar block copolymers the rubbery chains are more constrained than in the cylindrical one, in which they form a continuum. This affects their deformation at both length scales.

Acknowledgement The authors thank Center for University of Massachusetts and Industry Research on Polymers (CUMIRP) Cluster-M and Kraton Polymers U. S. LLC for their support and the National Science Foundation Materials Research Science and Engineering Center for their financial support.

References

1. Holden G, Legge NR, Quirk R, Schroeder HE (1996) Thermoplastic elastomers, 2nd edn. Hanser Publishers, Cincinnati
2. Honeker CC, Thomas EL (1996) Chem Mater 8:1702
3. Honeker CC, Thomas EL (2000) Macromolecules 33:9407
4. Honeker CC, Thomas EL, Albalak RJ, Hajduk DA, Gruner SM, Capel MC (2000) Macromolecules 33:9395
5. Yamaoka I, Kimura M (1993) Polymer 34:4399
6. Odell JA, Keller A (1977) Polym Eng Sci 17(8):544
7. Sakamoto J, Sakurai S, Doi K, Nomura S (1993) Polymer 34:4837
8. Seguela R, Prud homme J (1981) Macromolecules 14:197
9. Sakurai S, Momii T, Taie K, Shibayama M, Nomura S (1993) Macromolecules 26:485
10. Sakurai S, Kawada H, Hashimoto T (1993) Macromolecules 26:5796
11. Sakurai S, Sakamoto J, Shibayama M, Nomura S (1993) Macromolecules 26:3351
12. Pakula T, Saijo K, Kawai H, Hashimoto T (1985) Macromolecules 18:1294
13. Cohen Y, Albalak RJ, Dair BJ, Capel MS, Thomas EL (2000) Macromolecules 33:6502
14. Cohen Y, Brinkmann M, Thomas EL (2001) J Chem Phys 114(2):984
15. Keller A, Odell JA (1985) In: Folkes MJ (ed) Processing structure and properties of block copolymers. Elsevier Applied Science Publishers, p 29
16. Stribeck N, Buzdugan E, Ghioca P, Serban S, Gehrke R (2002) Macromol Chem Phys 203:636
17. Murthy NS, Grubb DT (2006) J Polym Sci [B] 44:1277
18. Tarasov SG, Tsvankin DY, Godovskii Yu K (1978) The structural changes during the deformation of orientated and isotropic butadiene-styrene block copolymers. Vysokomolekulyarnye Soedineniya Seriya A 20(7):1534
19. Read DJ, Duckett RA, Sweeney J, McLeish TCB (1999) J Phys D Appl Phys 32:2087
20. Sierra CA, Galan C, Fatou JG, Parellada MD, Barrio JA (1997) Polymer 38(17):4325
21. Indukuri KK, Lesser AJ (2005) Polymer 46:7218
22. Indukuri KK (2005) Polymer science and engineering. University of Massachusetts Amherst, Amherst
23. Lyon RE, Rabolin PJ (1995) J Therm Anal Calorim 44(4):777
24. Lyon RE, Rabolin PJ, (1984) Polymer science and engineering, University of Massachusetts Amherst, Amherst
25. Lyon RE, Farris RJ (1984) Polym Sci Eng 25:908
26. Lyon RE, Wang DX, Farris RJ, MacKnight WJ (1984) J Appl Polym Sci 29(9):2857
27. Shibayama M, Hashimoto T, Kawai H (1983) Macromolecules 16:16